Dissociation of B–H pairs in diamond as enhanced by electronic excitation and electron capture: Computational modeling

J. P. Goss and P. R. Briddon
School of Natural Sciences, University of Newcastle upon Tyne, Newcastle upon Tyne NE1 7RU, United Kingdom
(Received 24 May 2007; revised manuscript received 12 October 2007; published 28 January 2008)

Boron acceptors in diamond can be passivated with hydrogen, forming B_s–H pairs. Thermally, these pairs dissociate with an activation energy of 2.5 eV, but under an electron beam, near complete reactivation of previously passivated acceptors can be achieved at 100 K. We present the results of density functional simulations examining the effect of the addition of minority carriers to B_s–H pairs and show that electronic excitation and negative charging significantly lower the barrier to dissociation.

DOI: 10.1103/PhysRevB.77.035211 PACS number(s): 61.72.J−, 61.72.Bb, 71.20.Mq, 71.23.An

I. INTRODUCTION

Diamond, intrinsically an indirect wide-gap, electrically insulating material, can be made to conduct via doping with a somewhat limited range of impurities. In particular, to produce *p*-type diamond, boron acceptors can be incorporated in very high concentrations leading to metallic[1] and even superconducting[2] samples.

Although much theoretical analysis has been directed to the interaction of hydrogen with impurities in diamond,[3–8] the only convincing case linked to experimental evidence is the formation of boron-hydrogen (and boron-deuterium) pairs (B_s–H) which convert *p*-type samples into insulators.[9–13] The electrical passivation is observed by capacitance-voltage measurements,[10] Hall effect[12] or mapped onto the loss of electronic infrared transitions,[9,11] and the bound-exciton emission associated with the neutral acceptor.[13] To date, direct spectroscopic identification of B_s–H pairs, such as by observation of hydrogen-related local vibrational modes, has not be achieved.

The activation energy for the thermal release of H from B_s–H pairs has been measured experimentally to follow an Arrhenius process with a slope of 2.5 ± 0.2 eV,[14] requiring annealing well above room temperature. Calculated values range from good to fair agreement with this value,[8,14,15] but all studies recognize the barrier implies a very slow dissociation rate at room temperature and below.

Intriguingly, recent experiments show that under electron-beam irradiation, the rate of dissociation is significantly increased, and nearly complete reactivation of deuterium passivated boron acceptors is achieved at 100 K.[13] The reactivation is determined by the observation of the neutral acceptor bound-exciton emission in cathodoluminescence under weak excitation conditions (2 min at 2 nA). The model proposed to explain this observation involves the promotion of multiple vibrationally excited states via interactions with hot electrons. Thermal dissociation of $(B_s\text{–H})^0_{S=0}$ may be ruled out due to the low temperatures involved, and it is argued that electronic excitation is not a likely cause due to a strong electron current dependence, which is not seen in cases where electron excitation is believed to be in play.[16,17] The role of minority carriers remains unresolved experimentally, but forms a central aspect of this current, theoretical study.

We present here the results of local-spin-density-functional calculations regarding the properties of B_s–H pairs in the presence of ionizing conditions and electronic excitation. In Sec. II, we detail the computational method. We report the results of the simulations in Sec. III and present our conclusions in Sec. IV.

II. METHOD

Calculations were carried out using the local-spin-density-functional technique, implemented in AIMPRO.[18] To model the defects, 64 and 216 atom, cubic supercells of side length $2a_0$ or $3a_0$ have been used, and the calculations are performed using the calculated equilibrium lattice constant of bulk diamond. The Brillouin zone is sampled using the Monkhorst-Pack scheme,[19] generally with a mesh of $2\times2\times2$ special *k* points, although convergence has been checked by calculating total energies with a denser mesh for selected systems. Core electrons are eliminated by using norm-conserving pseudopotentials.[20]

The wave function basis consists of atom-centered Gaussians.[21] Carbon atoms are treated using linear combinations of *s* and *p* orbitals with the addition of *d* functions to allow for polarization. Boron and hydrogen are treated using four and three independent sets *s*- and *p*-Gaussians with four widths, respectively, with the addition of two sets of *d*-polarization functions for the B atoms. The charge density is Fourier transformed using plane waves with a cutoff of 300 Ry, yielding well converged total energies.

Using the above procedure, the lattice constant and bulk modulus of bulk diamond are reproduced to within ~1 and 5%, respectively, of experiment, while the direct and indirect band gaps at 5.68 and 4.26 eV, respectively, are close to previously published plane-wave values.[22]

The formation energy of X in charge state q is calculated using[23]

$$E^f(X,q) = E(X,q) - \sum \mu_i + q(E_v^X + \mu_e) + \chi(q), \qquad (1)$$

where E is the total energy, μ_i and μ_e are the chemical potentials of the atoms and electrons, respectively, E_v^X is the energy of E_v in the defect cell, and χ is the correction for periodic boundary conditions, for which we include only the Madelung term,[24] which for cubic supercells of side length

$2a_0$ and $3a_0$ is around $0.53q^2$ and $0.35q^2$ eV, respectively. The use of the Madelung energy to mitigate the problems inherent in the simulation of charged systems in periodic boundary conditions is a crude approach and will be an overestimate for systems which are delocalized. One can view the Madelung energy as an order of magnitude estimate of the error in the location of shallow electrical levels. Thus, donor or acceptor electrical levels may be estimated, at least qualitatively given the uncertainties in the charged cell energies, using the formation energy method.[25] Electrical levels calculated in this way are thermodynamic in nature and are not dependent on whether processes involve direct or indirect band gaps. The calculation of levels using the comparative marker method[21] is not applicable in the current study as there are no experimental data for acceptor levels close to the conduction band in this material.

We define a binding energy by

$$E^b(XY) = E^f(X) + E^f(Y) - E^f(XY), \quad (2)$$

so that a positive value represents a bound XY complex. Binding energies calculated this way include small errors arising from the cell size, the fixed-volume boundary condition, the application of charged-cell corrections, and those inherent to the underlying method. The magnitude of the error is hard to determine precisely, but we note that comparison of calculated and experimental values[14] for B_s–H yields an error bar of the order of 0.2 eV. Furthermore, by comparison of binding energies in the different cells, we also estimate that the binding energies to be converged to within this tolerance.

Finally, activation energies for atomic motion have been obtained using the climbing nudged-elastic-band (NEB) method.[26,27] Each diffusion process is modeled using 21 images. The saddle point structures are determined with a tolerance of less than 0.01 a.u. on the forces on each image. The dependence of the activation energies on cell size, Brillouin-zone sampling, plane-wave energy, and wave function basis have been assesses to have a combined effect of less than 0.1 eV.

III. RESULTS

We have calculated the properties and stability of H atoms located at bond-centered locations various distances from B_s. Examples of each of the six nearest bond-centered sites relative to boron are indicated schematically in Fig. 1. For each location of H, we relaxed a range of charge states from −2 to +1, as well as the $S=0$ and $S=1$ spin configurations of the neutral systems. The high-spin neutral configuration can be viewed as a computational mechanism for examining the properties of B_s^0–H_i^0 complexes, rather than B_s^-–H_i^+.

A. Geometry and electronic structure

We first review the properties of B_s–H pairs at sites 1 and 2 in Fig. 1. Nominally, we can treat B_s as possessing a single acceptor level close to the valence band top of diamond (E_v), whereas, at least theoretically, interstitial hydrogen possesses both donor and acceptor levels deep within the band gap.[5,8,28]

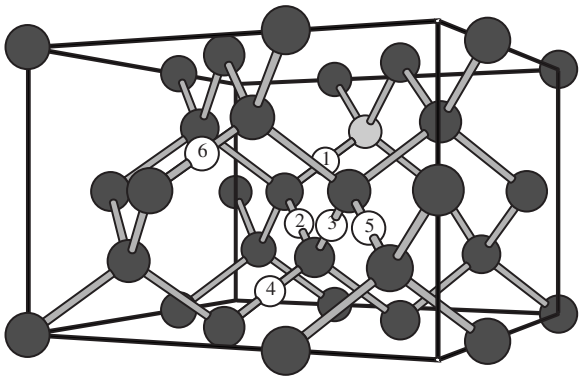

FIG. 1. Schematics of bond-centered sites relative to an on-site substitutional boron defect in diamond. Dark, light, and white atoms represent C, B, and bond-center sites for H_i, respectively. The enclosing box is aligned along the crystallographic [100], [010], and [001] directions.

Taking first the donor property of H_i, the formation of B_s–H pairs constitutes a simple donor-acceptor, B_s^-–H^+, complex corresponding to the passivated acceptor inferred from experiment.

The relaxed structure we obtain for $(B_s\text{–}H)^0_{S=0}$ at site 1 is shown in Fig. 2(a) and the corresponding band structure is plotted in Fig. 3(a). The three-member ring formed by B, H, and C is a characteristic of boron chemistry and has been examined in detail previously.[5] The structure may also be viewed as B_s^- and a perturbed H_i^+ center, which adopts a puckered bond-centered configuration.

For the reaction

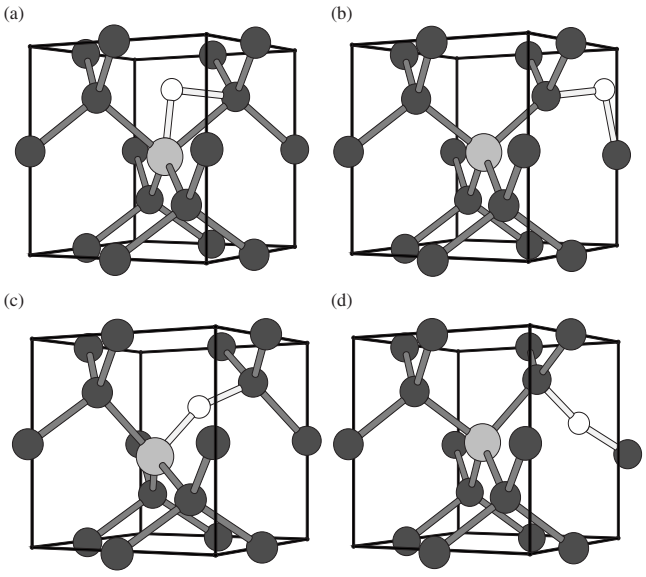

FIG. 2. Schematics of B_s–H complexes in diamond. White, dark, and light gray atoms are H, C, and B, respectively. The box indicates the underlying cubic axes of the diamond lattice. (a) and (b) show the geometries of neutral pairs at nearest and next-nearest sites, with (c) and (d) being for the negative charge state.

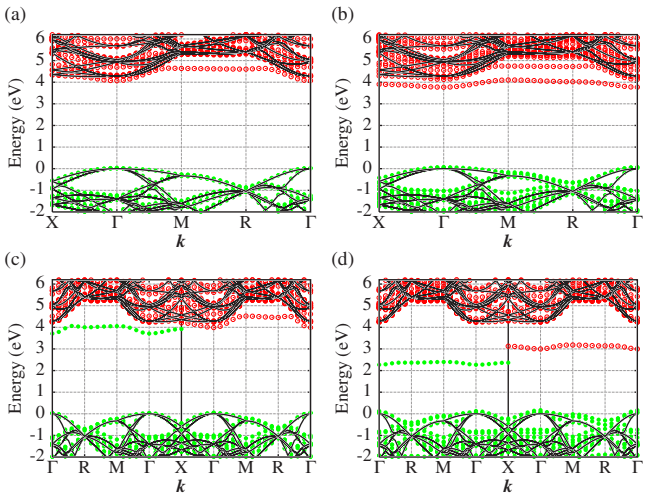

FIG. 3. (Color online) Kohn-Sham bands structures in the vicinity of the band gap along high-symmetry directions of the first Brillouin zone of a 216-atom supercell containing the structures shown in Fig. 2. Green (filled circles) show occupied levels and red (empty circles) empty bands. Black lines are bands for a defect-free cell, and the zero of energy is defined as the valence band top of diamond. In (c) and (d), the left and right panels show the spin up and down spectra, respectively.

$$(\mathrm{B}_s - \mathrm{H})^0_{S=0} + e^- \rightarrow (\mathrm{B}_s - \mathrm{H})^-$$

to be able to occur in equilibrium, the B_s–H complex must possess an acceptor level. The band structure, shown in Fig. 3(a), suggests this is not the case, and there are no donor or acceptor levels in the theoretical band gap, as determined from the charge-dependent formation energies and plotted in Fig. 4(a). Due to the uncertainty inherent of the method, principally due to the charge-charge interactions in the periodic boundary conditions and perhaps due to the underestimate in the band gap, the estimate of an acceptor level just above the conduction band minimum does not rule out the capture of an electron by B_s–H. Indeed, Fig. 3(a) indicates the presence of a dispersionless empty band above the conduction band minimum, which is localized on the hydrogen atom and the carbon and boron atoms which the hydrogen neighbors.

We find that placing an additional electron to form $(B_s\text{–H})^-$ system pushes the H atom onto the bond center [Fig. 2(c)] and occupies a highly localized antibonding orbital with a node around the location of the H atom. The character of the unpaired electron is reminiscent of that of isolated H_i^0, which is an axial center in contrast to puckered bond of the positively charged interstitial hydrogen.

Since H_i possesses deep donor and acceptor levels,[5,8,28] it must be the case that there is an acceptor level for a pair of B_s and H_i systems if they are sufficiently separated one from the other that the interaction is negligible. Indeed, this is what we find to be the case, so that even displacing H from site 1 to site 2 results in $(B_s\text{–H})^-$ possessing a geometry [Fig. 2(d)] and electronic structure [Fig. 3(d)] closely related to H_i^0. At site 2, $(B_s\text{–H})^-$ is thermodynamically stable for an electron chemical potential in the upper half of the band gap, as shown in Fig. 4(b).

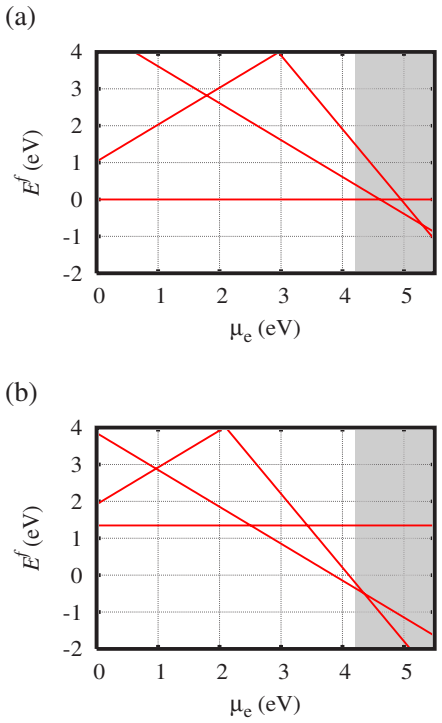

FIG. 4. (Color online) Formation energies (E^f) for B_s–H complexes with H at sites (a) 1 and (b) 2, as shown in Fig. 1. The slope of each line indicates the charge and the shaded area indicates the region between the theoretical and experimental band gaps. The valence band top is at $\mu_e=0$ eV, and the formation energies are computed using Eq. (1) with μ(atom) taken such that $E^f[(B_s\text{–H})^0, \text{site } 1, S=0]=0$ eV.

Since $(B_s\text{–H})^0_{S=1}$ can be viewed as B_s^0–H_i^0, it is unsurprising that this configuration closely matches $(B_s\text{–H})^-$ in geometry and electronic structure with the addition of a hole in a band close to E_v. Figure 4(b) also suggests that a *double acceptor* level may be present, albeit very high in the band gap. $(B_s\text{–H})^{2-}$ may be viewed as B_s^-–H_i^-.

B. Energetics for dissociation

Varying the starting location of the bond center containing H in line with Fig. 1, we have obtained energy profiles for the five electronic configurations, and we plot the results in Fig. 5. The total energies are reduced with increasing distance for systems where the hydrogen component may be considered as H_i^0 or H_i^-, i.e., $(B_s\text{–H})^0_{S=1}$, $(B_s\text{–H})^-$, and $(B_s\text{–H})^{2-}$. In contrast, the total energies increase for $(B_s\text{–H})^0_{S=0}$ and $(B_s\text{–H})^+$.

We may make a number of observations. First, for $(B_s\text{–H})^-$ and $(B_s\text{–H})^0_{S=1}$, one or both of the dissociated products are charge neutral, so that there is no long range Coulomb contribution to the binding energy. The variation in total energy with displacement for sites 2–6 is modest with 0.2 eV covering all values.

For $(B_s\text{–H})^0_{S=0}$ and $(B_s\text{–H})^{2-}$, the dissociated products are both charged, and the energy profiles include long-range at-

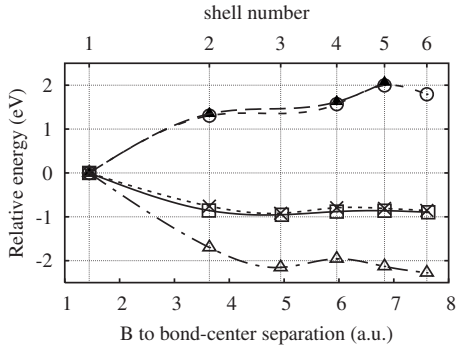

FIG. 5. Optimized total energy (eV) relative to site 1 (Fig. 1) versus bond-center site for B_s–H pairs in different spins and charge states: ○, $(B_s\text{–}H)^+$; ▲, $(B_s\text{–}H)^0_{S=0}$ $(S=0)$; □, $(B_s\text{–}H)^0_{S=1}$; ×, $(B_s\text{–}H)^-$; and △, $(B_s\text{–}H)^{2-}$. The shell numbers refer to Fig. 1, and the distances are for the ideal, unrelaxed bond-centered location. The lines linking the data are included as a guide to the eye and, in particular, do not represent the barriers to interconversion.

tractive and repulsive Coulomb terms, respectively.

The calculated binding energies for the five systems plotted in Fig. 5 are 1.9, 2.7, −0.8, −0.8, and −2.9 eV for $(B_s\text{–}H)^+$, $(B_s\text{–}H)^0_{S=0}$, $(B_s\text{–}H)^0_{S=1}$, $(B_s\text{–}H)^-$, and $(B_s\text{–}H)^{2-}$, respectively. We shall return to these asymptotic values in the following section, but we note that for $(B_s\text{–}H)^{2-}$ and $(B_s\text{–}H)^0_{S=0}$, the energies in Fig. 5 are not converged for the most distant pairs, whereas for $(B_s\text{–}H)^0_{S=1}$ and $(B_s\text{–}H)^-$, the values are close to the binding energies even at site 2.

It is also clear that the energy profiles for $(B_s\text{–}H)^0_{S=1}$ and $(B_s\text{–}H)^-$ are closely matched. This may be due to the delocalized nature of the boron acceptor in $(B_s\text{–}H)^0_{S=1}$ contributing relatively little to the interaction between the two impurities. A similar argument applies to comparison of $(B_s\text{–}H)^0_{S=0}$ and $(B_s\text{–}H)^+$.

C. Kinetics

Figure 5 clearly indicates that upon excitation or capture of electrons there exists a driving force to dissociate B_s–H pairs. The data points in this plot represent local minima in the energy surface, and between each of these there will, in general, exist barriers to diffusion that will play a role in the kinetics of dissociation. In order to shed some light upon these barriers, we have calculated the activation energy for the first step, i.e., site 1 to site 2 in Fig. 1, for each electronic configuration.

For the three configurations that are unbound, the dissociation mechanisms that we have modeled are very similar, and we detail here only that of the negatively charged system. The path involves motion between structures (a) and (e) in Fig. 6. The barrier to interconversion obtained using the NEB approach results in the formation of another metastable structure, shown in Fig. 6(c). This structure, where the hydrogen atom is in a nonbonded, approximately tetrahedral interstitial location, suggests a two stage migration that is activated by around 0.6 eV. The diffusion energy profile, shown in Fig. 6, is clearly lower than the energy required to dissociate the neutral impurity pair.

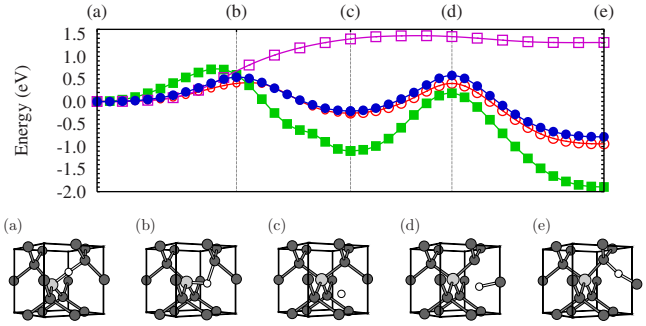

FIG. 6. (Color online) NEB diffusion barriers for dissociation of B_s–H pairs. Filled circles (blue): $(B_s\text{–}H)^-$; empty circles (red): $(B_s\text{–}H)^0_{S=1}$; filled squares (green): $(B_s\text{–}H)^{2-}$; and empty squares (magenta): $(B_s\text{–}H)^0_{S=0}$, $S=0$. Structures (a)–(e) are for the (meta)stable and transition states for $(B_s\text{–}H)^-$.

For kinetic barriers, the above simulations have been performed using the smaller cell containing 64 host sites due to the computational cost of these simulations. For $(B_s\text{–}H)^-$, we repeated the simulations using the larger computational cell, obtaining a similar barrier of 0.7 eV. We also examined the role of basis for the smaller cell and found that increasing the number of basis functions also had only a very modest effect on the barrier heights and profiles. We therefore conclude that the results presented in Fig. 6 are sufficiently converged.

Qualitatively, the same two-stage dissociation process is found for $(B_s\text{–}H)^0_{S=1}$ and $(B_s\text{–}H)^{2-}$, the NEB profiles for which are also plotted in Fig. 6. The maxima calculated for these electronic configurations are 0.5 and 0.7 eV, respectively.

For $(B_s\text{–}H)^0_{S=1}$, $(B_s\text{–}H)^-$, and $(B_s\text{–}H)^{2-}$, the nonbonded hydrogen [Fig. 6(c)] represents a local minimum in total energy, but this is not the case for the neutral and positively charged systems, where starting from this structure leads to a spontaneous relaxation to site 1. The barrier obtained for $(B_s\text{–}H)^0_{S=0}$ is also plotted in Fig. 6 for comparison. This first step in thermal dissociation has a barrier of around 1.5 eV, around 55% of the calculated binding energy. The remainder of the barrier to full dissociation arises from overcoming the Coulomb attraction between B_s^- and H_i^+ to large separations.

It is important to relate the first step to the overall dissociation where the boron and hydrogen components are separated to large distances. To this end, we note that the calculated barriers to migration for H_i^0 and H_i^- in bulk diamond are around 1.6 and 2.0 eV, respectively.[29] The energy for $(B_s\text{–}H)^-$ at site 2 is 0.9 eV below that of site 1 (Fig. 5). Assuming the migration barrier of H_i^0 to be that of isolated H_i between sites 2 and 3, viz., 1.6 eV, this places the diffusion barrier at around 0.7 eV relative to site 1. Thus, the activation energy for dissociation to large distances for $(B_s\text{–}H)^-$, $(B_s\text{–}H)^{2-}$, and $(B_s\text{–}H)^0_{S=1}$ are close to the barriers shown in Fig. 6, i.e., 0.5–0.7 eV. We explore this further in Sec. III D.

In contrast to thermal processing,[30] diffusion is unlikely to be trap limited for electron rich systems. This is because under the electron beam B_s will most probably be ionized, and since $(B_s\text{–}H)^-$ is unbound it will not be a trapping site.

Indeed, the presence of a negative charge may contribute to a field enhanced migration, as proposed for athermal displacement of lattice damage in diamond under irradiation from an electron beam.[31]

For a Boltzmann process to yield a hop rate of the order of 1 Hz, presupposing an attempt frequency of 40 THz,[32] suggests a barrier of around 0.3 eV corresponds to the experimental temperature of 100 K. The barrier heights calculated between 0.5 and 0.7 eV clearly exceed this value. However, they are classical in nature, and it is known that quantum effects may be important for hydrogen containing systems in diamond.[33] Indeed, the calculated classical barrier to reorientation for vacancy-nitrogen-hydrogen complexes is very similar at 0.4 eV, but the experimental observations are consistent with H tunneling between sites at low temperature.[34] Furthermore, we have prescribed the route for diffusion to involve insertion into site 2 in Fig. 1. Therefore, the barriers can generally be taken to be upper bounds and may be viewed as consistent with thermal dissociation at 100 K. It may be that repeating the experiments at lower temperatures would help shed light on the upper bound to thermal processes accounting for the observations.

Regrettably, the current computational method is not able to comment upon a multivibrational mode process for the enhanced dissociation of B_s–H pairs under an electron beam. However, the calculations show that irrespective of the role of vibrational excitation, a high density of minority carrier would lead to dissociation at lower temperatures than in their absence.

D. Fate of the hydrogen

The question of the destination of the hydrogen or deuterium after release from the B_s–H and B_s-D pairs remains open. We note that an individual H_i is a deep electron donor, and would therefore be expected to compensate the boron acceptors in thermodynamic equilibrium. We present three possible schemes that would be consistent with the experimental observations.

(a) H_i released from B_s–H complexes end up in passive complexes containing an even number of hydrogen atoms.

(b) H_i are unable to compensate the acceptors due to their distance from them, i.e., thermodynamic equilibrium is not achieved, which is feasible in diamond as an electrical insulator.[35]

(c) H_i are completely lost from the region of material where the cathodoluminescence related boron bound-exciton emission originates.

For (a), we have examined the energetics for reactions involving B_s–H complexes and hydrogen aggregates. The most stable form of hydrogen dimer is H_2^*,[5,36] but larger aggregates, such as a pair of these centers[29] (H_4) is even more stable. The reactions are

$$(B_s - H)^0_{S=0} \rightarrow B_s^0 + \frac{1}{2}H_2^* - 2.4 \text{ eV},$$

$$(B_s - H)^0_{S=0} \rightarrow B_s^0 + \frac{1}{4}H_4 - 1.8 \text{ eV},$$

which are endothermic. However, in the presence of minority carriers, the reactions of interest may be of the form

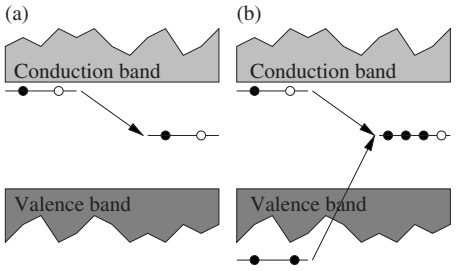

FIG. 7. Schematic of the change in gap levels associated with the dissociation of (a) $(B_s$–$H)^-$ and (b) $(H_2^*)^-$. Black and white circles represent filled and empty levels, respectively.

$$(B_s - H)^- \rightarrow B_s^- + \frac{1}{2}H_2^* + 2.1 \text{ eV},$$

$$(B_s - H)^- \rightarrow B_s^- + \frac{1}{4}H_4 + 2.6 \text{ eV},$$

which are exothermic. Indeed, these reactions liberate so much energy that they are exothermic relative to dissociated B_s–H pairs. This suggests that in the presence of excess electrons there is a energetic benefit in the formation of hydrogen aggregates such as H_2^*.

Once the electron beam is removed, although thermodynamic equilibrium would tend to dissociate the hydrogen complexes to reform B_s–H pairs, the considerable binding energy of H_2^* and H_4 aggregates (1.3 and 1.8 eV/H atom, respectively) would prevent this from happening unless the material is annealed. Aggregates of even numbers of H atoms are electrically passive, and the formation of H_2^* and H_4 or similar systems would therefore lead to the reactivation of B_s, as observed experimentally. This model relies on the behavior of electrically passive H_2^* being qualitatively different from that of electrically passive B_s–H, i.e., that H_2^* cannot become negatively charged.

Indeed, this is what we find. During the dissociation of $(B_s$–$H)^-$ into B_s^- and H_i^0, a shallow partially filled level moves to midgap [Figs. 3(b) and 3(d)]. The midgap state associated with H_i^0 contains a single electron, shown schematics in Fig. 7(a). In the case of dissociation of $(H_2^*)^-$, shown schematically in Fig. 7(b), two interstitial hydrogen species are formed, and their two midgap levels contain *three* electrons. In this simple picture, there is an energy saving in the $(B_s$–$H)^-$ case related to the lowering in the gap of the half-filled level, and a cost for $(H_2^*)^-$ since two filled states are pushed up in energy, and only one moves down. The calculations show that separate H_i^0 and H_i^- is higher in energy than H_2^* and an electron in the conduction band by 0.5 eV in a 216 atom supercell. Therefore, in contrast to what we find for B_s–H, there is no energetic reason for the dissociation of H_2^* to proceed under the injection of minority carriers. Thus, the formation of passive hydrogen aggregates, irreversible at the low experimental temperatures, is a plausible explanation for the reactivation of B_s.

As mentioned above, migration of H_i^0 is an activated process and should not occur rapidly at 100 K. The question is

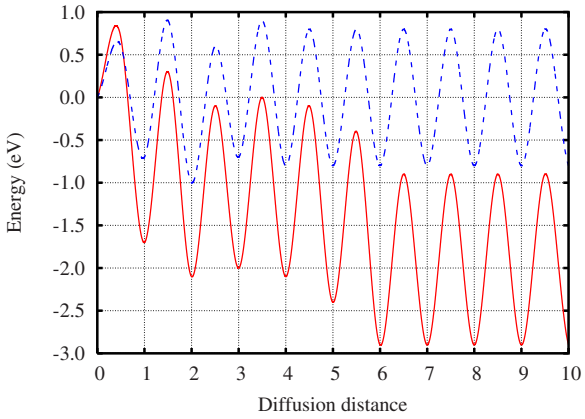

FIG. 8. (Color online) Schematic representations of the energy profiles for diffusion of H_i^0 (dashed line) and H_i^- (solid line) in the dissociation of $(B_s\text{–}H)^-$ and $(B_s\text{–}H)^{2-}$, respectively. Diffusion distance is in units of atomic steps. Barriers beyond the first step is assumed to be that in bulk (1.6 and 2.0 eV for H_i^0 and H_i^-, respectively). Minima from step 6 onward are based on the overall binding energies of −0.8 and −2.9 eV.

whether the energy supplied to B_s–H by the absorption of an electron is sufficient to allow the released H_i^0 to migrate far enough to be captured by another H_i^0. The calculations suggest that the first step is on a par with the overall barrier, as illustrated schematically in Fig. 8. During migration, H_i^0 would lose energy in the form of lattice phonons. Once the kinetic energy of is sufficiently reduced, the hydrogen will be trapped in a bond center.

A problem then arises. If the diffusion distance of H_i^0 is small, then they will not be able to form aggregates and hence would be electrically active. If this is the case and hydrogen is dissolved in the material as individual H_i^0, but they are sufficiently far from any B_s, they may not be able to donate their electrons to compensate B_s^0 once the electron beam is removed. This is case (b). Assuming that effective mass theory adequately represents the acceptor wave function of B_s, one can estimate the orbit to have a radius of 3–8 Å,[37] which is fewer than three lattice constants. The donor wave function of H_i^0 is midgap and highly localized, and its extent can be ignored. Thus, if all H_i diffuse to a distance in excess of the effective Bohr orbit from any B_s^- under the electron beam, the material may appear as if the hydrogen has been lost with respect to the boron related optical emission.

The diffusion length of H_i subsequent to dissociation may not be so limited if during electron irradiation continuous excitation of H_i may drive its migration, in line with the model of Barjon *et al.*[13] Indeed, excitation via an electron beam is thought to be the cause of athermal motion of self-interstitials in diamond. In this case, the thermal barrier to migration is close to 1.6–1.7 eV,[38,39] but during electron irradiation at cryogenic temperatures, they can aggregate to form the R1 and O3 EPR centers.[40]

Finally, we examine case (c). If during electron irradiation the released hydrogen is predominantly negatively charged (H_i^-), then the formation of hydrogen aggregates would be inhibited due to mutual Coulomb repulsion. However, the accumulation of negative charge within the irradiation region would lead to an electric field which could enhance the migration of H_i^- away from the electron beam, as suggested for charged lattice damage species.[31] If this is the principal mechanism, then the irradiated region would have very low hydrogen densities in comparison to the surrounding material. This would be in contrast to a mechanism involving hydrogen aggregate formation, which would maintain a constant average hydrogen density throughout the material.

IV. CONCLUDING REMARKS

We have modeled the energetics of dissociation of B_s–H pairs in diamond under the assumption that during excitation, such as provided by an electron beam, nonequilibrium charge and spin state may be populated.

Of the candidate electronic configurations examined, $(B_s\text{–}H)^0_{S=1}$ $(B_s\text{–}H)^-$, and $(B_s\text{–}H)^{2-}$ cases all show a reduction in the barrier to dissociation relative to that of $(B_s\text{–}H)^0_{S=0}$. The barriers of 0.5–0.7 eV are likely to be upper bounds since the effective barriers including quantum tunneling effects will be lower, as proposed for H hopping within vacancies.[33,34]

We suggest that excitation and minority carrier capture processes may be the underlying processes involved in the enhanced dissociation seen in experiment using electron beams.[13] If, as we find, the barrier is reduced sufficiently upon charging, the subsequent reactivation of B_s^0 acceptors may be considered an entirely thermal process. However, it cannot be determined what role, if any, the vibrational excitation of the hydrogen may have, and it might be that a combination of electronic and vibrational effects are in play.

Of the possible end product of the hydrogen lost from the B_s–H complexes, the simple explanations involving the migration of H_i outside the region investigated via the CL experiment or the formation of electrically inactive dimers are both reasonable candidates. Clarification from further experiment is needed, and we suggest that determination of effects at lower temperatures, and the spatial distribution of hydrogen subsequent to reactivation of the acceptors would be highly desirable experiments in order to further specify the underlying processes.

ACKNOWLEDGMENTS

We gratefully acknowledge discussions with J. Chevallier and J. Barjon, as well as funding provided by EPSRC, UK.

[1] K. Thonke, Semicond. Sci. Technol. **18**, S20 (2003).
[2] E. A. Ekimov, V. A. Sidorov, E. D. Bauer, N. N. Mel'nik, N. J. Curro, J. D. Thompson, and S. M. Stishov, Nature (London) **428**, 542 (2004).
[3] T. Miyazaki, H. Okushi, and T. Uda, Appl. Phys. Lett. **78**, 3977 (2001).
[4] T. Nishimatsu, H. Katayama-Yoshida, and N. Orita, Physica B **302-303**, 149 (2001).
[5] J. P. Goss, R. Jones, M. I. Heggie, C. P. Ewels, P. R. Briddon, and S. Öberg, Phys. Rev. B **65**, 115207 (2002).
[6] T. Miyazaki, H. Okushi, and T. Uda, Phys. Rev. Lett. **88**, 066402 (2002).
[7] T. Nishimatsu, H. Katayama-Yoshida, and N. Orita, Jpn. J. Appl. Phys., Part 1 **41**, 1952 (2002).
[8] T. Cai, Y. Zhang, A. B. Anderson, J. C. Angus, and T. V. Kostadinov, and L. N. abd Albu, Diamond Relat. Mater. **15**, 1868 (2006).
[9] J. Chevallier, B. Theys, A. Lusson, C. Grattepain, A. Deneuville, and E. Gheeraert, Phys. Rev. B **58**, 7966 (1998).
[10] R. Zeisel, C. E. Nebel, and M. Stutzmann, Appl. Phys. Lett. **74**, 1875 (1999).
[11] Z. Teukam, J. Chevallier, C. Saguy, R. Kalish, D. Ballutaud, M. Barbé, F. Jomard, A. Tromson-Carli, C. Cytermann, J. E. Butler, M. Bernard, C. Baron, and A. Deneuville, Nat. Mater. **2**, 482 (2003).
[12] N. Ogura, M. Mizuochi, S. Yamasaki, and H. Okushi, Diamond Relat. Mater. **14**, 2023 (2005).
[13] J. Barjon, J. Chevallier, F. Jomard, C. Baron, and A. Deneuville, Appl. Phys. Lett. **89**, 232111 (2006).
[14] J. P. Goss, P. R. Briddon, R. Jones, Z. Teukam, D. Ballutaud, F. Jomard, J. Chevallier, M. Bernard, and A. Deneuville, Phys. Rev. B **68**, 235209 (2003).
[15] E. B. Lombardi, A. Mainwood, and K. Osuch, Phys. Rev. B **70**, 205201 (2004).
[16] T.-C. Shen, C. Wang, G. C. Abein, J. R. Tucker, J. W. Lyding, Ph. Avouris, and R. E. Walkup, Science **268**, 1590 (1995).
[17] J. Chevallier, M. Barbé, E. Constant, D. Loridant-Bernard, and M. Constant, Appl. Phys. Lett. **75**, 112 (1999).
[18] R. Jones and P. R. Briddon, in *Identification of Defects in Semiconductors*, Semiconductors and Semimetals Vol. 51A, edited by M. Stavola (Academic, Boston, 1998), Chap. 6.
[19] H. J. Monkhorst and J. D. Pack, Phys. Rev. B **13**, 5188 (1976).
[20] C. Hartwigsen, S. Goedecker, and J. Hutter, Phys. Rev. B **58**, 3641 (1998).
[21] J. P. Goss, M. J. Shaw, and P. R. Briddon, in *Theory of Defects in Semiconductors*, Topics in Applied Physics Vol. 104, edited by David A. Drabold and Stefan K. Estreicher (Springer, Berlin, 2007), pp. 69-94.
[22] D. A. Liberman, Phys. Rev. B **62**, 6851 (2000).
[23] S. B. Zhang and J. E. Northrup, Phys. Rev. Lett. **67**, 2339 (1991).
[24] G. Makov and M. C. Payne, Phys. Rev. B **51**, 4014 (1995).
[25] J. P. Goss, P. R. Briddon, S. J. Sque, and R. Jones, Diamond Relat. Mater. **13**, 684 (2004).
[26] G. Henkelman, B. P. Uberuaga, and H. Jónsson, J. Chem. Phys. **113**, 9901 (2000).
[27] G. Henkelman and H. Jónsson, J. Chem. Phys. **113**, 9978 (2000).
[28] L. G. Wang and A. Zunger, Phys. Rev. B **66**, 161202(R) (2002).
[29] J. P. Goss, J. Phys.: Condens. Matter **15**, R551 (2003).
[30] Z. Teukam, D. Ballutaud, F. Jomard, J. Chevallier, M. Bernard, and A. Deneuville, Diamond Relat. Mater. **12**, 647 (2003).
[31] J. W. Steeds, S. J. Charles, J. Davies, and I. Griffin, Diamond Relat. Mater. **9**, 397 (2000).
[32] 40 THz is an approximate value of the Raman frequency of diamond. The precise value used for the attempt frequency is less important than its order of magnitude since the activation energy depends upon it logarithmically.
[33] M. J. Shaw, P. R. Briddon, J. P. Goss, M. J. Rayson, A. Kerridge, A. H. Harker, and A. M. Stoneham, Phys. Rev. Lett. **95**, 105502 (2005).
[34] J. P. Goss, P. R. Briddon, R. Jones, and S. Sque, J. Phys.: Condens. Matter **15**, S2903 (2003).
[35] A. T. Collins, J. Phys.: Condens. Matter **14**, 3743 (2002).
[36] P. Briddon, R. Jones, and G. M. S. Lister, J. Phys. C **21**, L1027 (1988).
[37] C. E. Nebel and M. Stutzmann, in *Properties, Growth and Applications of Diamond*, EMIS Datareviews Series No. 26, edited by M. H. Nazaré and A. J. Neves (INSPEC, Institute of Electrical Engineers, London, 2001), Chap. A1.6, pp. 40–52.
[38] L. Allers, A. T. Collins, and J. Hiscock, Diamond Relat. Mater. **7**, 228 (1998).
[39] D. J. Twitchen, D. C. Hunt, C. Wade, M. E. Newton, J. M. Baker, T. R. Anthony, and W. F. Banholzer, Physica B **273-274**, 644 (1999).
[40] D. J. Twitchen, D. C. Hunt, M. E. Newton, J. M. Baker, T. R. Anthony, and W. F. Banholzer, Physica B **273-274**, 628 (1999).